

Three-dimensional velocity field for wavy Taylor–Couette flow

Alp Akonur^{a)} and Richard M. Lueptow

Department of Mechanical Engineering, Northwestern University, Evanston, Illinois 60208

(Received 13 September 2002; accepted 3 January 2003; published 4 March 2003)

The stability of wavy supercritical cylindrical Couette flow has been studied extensively, but few measurements of the velocity field in flow have been made. Particle image velocimetry was used to measure the azimuthal and radial velocities in latitudinal planes perpendicular to the axis of rotation for wavy cylindrical Couette flow in the annulus between a rotating inner cylinder and a fixed outer cylinder. These measurements were matched to previous measurements of the axial and radial velocity measured in several meridional planes resulting in an experimentally measured, time-resolved, three-dimensional, three-component velocity field for wavy cylindrical Couette flow. Using this complete velocity field it is possible to evaluate details of the flow field. The vortical motion transports azimuthal momentum radially while the axial exchange of fluid between vortices in wavy flow transports azimuthal momentum axially. As the Reynolds number increases, these effects strengthen. Streams of net axial flow stretch axially along the length of the annulus and wind around the vortices from the inner cylinder to the outer cylinder and back while also winding azimuthally in the annulus. The azimuthal velocity measured at the center of a vortex is similar to the azimuthal wave speed. Measurements of the azimuthal velocity in cylindrical surfaces concentric with the axis of rotation suggest that the origin of the waviness is related to a jet-like azimuthal velocity profile rather than the radial outflow jet. Near both cylinder walls, the shear stress is quite large, decreasing to near zero at the middle of the annular gap. © 2003 American Institute of Physics. [DOI: 10.1063/1.1556615]

I. INTRODUCTION

Since Taylor's pioneering experiments and analysis,¹ supercritical cylindrical Couette flow has been studied in great detail.^{2–5} Most research has been directed toward the stability of the flow with only minor attention to the supercritical velocity field that develops in the annulus. Nevertheless, an understanding of the velocity field is crucial to engineering applications of the flow such as Couette mixing devices and rotating filter separators.

A limited number of measurements of the velocity have been made at single points in vortical nonwavy cylindrical Couette flow. Gollub and Freilich and Berland *et al.* measured the radial velocity (v_r) at a fixed radial position and several axial positions using laser Doppler velocimetry (LDV).^{6,7} Heinrichs *et al.* used LDV to measure the axial velocity (v_z) in Taylor vortex flow at a series of points distributed in the axial direction for a fixed radial position.⁸ Wereley and Lueptow generated contour plots of the azimuthal velocity (v_θ) based on extensive LDV measurements over a two-dimensional (r,z) grid of about 300 points per vortex pair.⁹ All of these LDV measurements were used to confirm the validity of Davey's perturbation expansion of the Navier–Stokes equations about the cylindrical Couette flow solution,¹⁰ particularly that the vortices strengthen with increasing rotating Reynolds number, $Re = r_i \Omega d / \nu$, where Ω is the angular velocity of the inner cylinder, $d = r_o - r_i$ is the gap between the outer cylinder of radius r_o and the inner

cylinder of radius r_i , and ν is the kinematic viscosity. Wereley and Lueptow measured the radial and axial velocities in a meridional plane for nonwavy Taylor vortex flow using particle image velocimetry (PIV).¹¹ Davey's theoretical velocity field matched their experimentally measured velocity quite well. From their measurements, Wereley and Lueptow were able to calculate the azimuthal component of velocity to provide all three components of the velocity field for this axisymmetric flow.

Wavy vortex flow in a cylindrical Couette device is substantially more complex than nonwavy flow. Flow visualization of wavy vortex flow suggests a stack of closed cell vortices that undulate with identical phase. However, the flow field is much more complicated than this.¹¹ The vortex centers (defined as the point within a vortex where the axial and radial velocities vanish in a meridional plane) have radial undulations in addition to moving axially. There is cyclic transport of significant quantities of fluid between vortices. In addition, local regions of net axial flow exist in parallel axial bands in the annulus coinciding with the wavy structure. Furthermore, the flow field is unsteady and fully three-dimensional (three components of velocity and three nonzero gradients of velocity), compared to nonwavy Taylor vortex flow, which is steady and has only two nonzero gradients.

Wavy vortex flow is also complicated in that the flow state is nonunique. Coles showed that a multiplicity of wavy vortex flow states differing in axial wavelength and the number of azimuthal waves around the annulus can occur for a given Reynolds number.¹² While nonlinear theory has been used to successfully predict the onset of waviness, the physi-

^{a)}Currently at Baxter Healthcare Corporation, Round Lake, IL 60073.

cal mechanism responsible for azimuthal waviness has been the subject of surprisingly little inquiry. Marcus suggested that a local, inviscid centrifugal instability of the radial outflow jet is responsible for the azimuthal waviness.¹³ However, Jones noted that the radial outflow jet results in strong azimuthal jets at the outflow region as it carries high azimuthal momentum outward.¹⁴ These azimuthal jets are much stronger than the radial jets that create them. Jones suggests that it is the azimuthal jets that destabilize the flow making the vortices wavy. Coughlin and Marcus concluded that in either scenario, radial jet or azimuthal jet, the important features related to waviness are at the outflow jet where both the radial and azimuthal velocities as well as the axial gradient of the azimuthal velocity are greatest.¹⁵

Few measurements of the velocity field for higher-order supercritical cylindrical Couette flow regimes have been made. These measurements are substantially more difficult because of the temporal and spatial dependence of the velocity field. Gollub and Swinney and Brandstater and Swinney measured the time dependence of the radial velocity (v_r) at a single location in the annulus for a large range of Reynolds numbers using LDV to demonstrate that the Landau picture of the transition to turbulence is not accurate and to determine that the attractor dimension is two for wavy vortex flow.^{16,17} Wereley and Lueptow used LDV to measure the two-dimensional (r,z) spatial distribution of the time-averaged azimuthal velocity (v_θ) for wavy, modulated wavy, and turbulent vortex flow.⁹ They found that the magnitude of the radial gradient of azimuthal velocity increases near both the inner and outer cylinders and that the radial outflow region between adjacent vortices becomes more jet-like as the Reynolds number increases. A small number of space-time measurements of wavy vortex flow have been made. Takeda *et al.* used an ultrasonic Doppler method to measure the space-time (z,t) dependence of a single velocity component (v_z) in wavy vortex flow.¹⁸ Ultrafast nuclear magnetic resonance imaging was used by Kose to measure the two-dimensional space (r,z) dependence of a single velocity component (v_r) for wavy vortex flow, but the sampling rate was too slow to adequately resolve the time dependence of the flow.¹⁹ Only the PIV measurements by Wereley and Lueptow provided temporal as well as two-dimensional spatial dependence (r,z,t) for two velocity components (v_r, v_z).¹¹ From these measurements, they found, among other things, that (1) vortex centers move radially as well as axially in the annulus; (2) cyclic transfer of a significant volume of fluid between vortices occurs; and (3) regions of local net axial flow corresponding to the axial deformation of the wavy vortex tube appear. As will be explained later in this paper, these measurements of the wavy velocity field in a meridional plane were combined with our new PIV measurements in a latitudinal plane (perpendicular to the axis of rotation) to provide a complete time-dependent, three-dimensional velocity field for all three velocity components.

Numerical simulations of Taylor vortex flow and wavy vortex flow have been successful in providing limited information about the velocity field.^{13,14,20–30} However, most of these studies focused on the computational methods, were aimed at very specific cases, modeled nonphysical condi-

tions, or provided minimal information about the velocity field. Marcus' detailed results and analysis are a notable exception.¹³ Unfortunately, several of these studies provide results for nonphysical situations such as wavelengths that are quite different from those seen experimentally or single wave situations, which occur quite infrequently.

Except for the PIV measurements of Wereley and Lueptow,¹¹ the measurements of the velocity field for cylindrical Couette flow have been quite limited in scope. Even these PIV measurements only provide two components of the velocity field. In this paper we present measurements of the third velocity component. Specifically, we present here time-resolved two-dimensional (r,θ,t) measurements of both the radial and azimuthal velocities (v_r, v_θ) as a function of Reynolds number for wavy vortex flow with the inner cylinder rotating and the outer cylinder fixed. These measurements are combined with Wereley and Lueptow's equivalent time-resolved two-dimensional (r,z,t) measurements of the radial and axial velocities (v_r, v_z) to provide a complete time-resolved, three-dimensional, three-component velocity field for typical wavy vortex flows at three Reynolds numbers.

The particle image velocimetry (PIV) measurements of the velocity field for supercritical cylindrical Couette flow described in this paper were aimed toward several objectives. The first objective was to accurately measure the remaining component of the velocity field in wavy vortex flow at several Reynolds numbers. The second objective was to examine the space- and time-dependence of the complete velocity field for a typical wavy vortex flow. The third objective was to determine the degree to which azimuthal momentum is transferred via the vortical motion and how this affects the velocity field as well as the shear stress distribution. The final objective was to provide the complete velocity field for typical wavy vortex flows for comparison to theory and computations. Although the emphasis here is on understanding the structure of wavy vortex above the transition from non-wavy to wavy vortex flow, we briefly consider issues related to the physical origin of the waviness.

II. EXPERIMENTAL METHODS

The flow cell used for the experiments was nearly identical to that used by Wereley and Lueptow.¹¹ It consisted of a pair of concentric acrylic cylinders, the inner one rotating and the outer one fixed. The inner cylinder had a radius of $r_i=4.24$ cm and the outer cylinder had a radius of $r_o=5.21$ cm resulting in a gap width of $d=0.97\pm 0.002$ cm and a radius ratio of $\eta=r_i/r_o=0.81$. The two cylinders were held concentric by aluminum endcaps, which also provided the fixed-end boundary conditions at the two axial extremes of the annulus. The lower endcap had a clear acrylic window to permit observation of laser-sheet-illuminated planes, which were perpendicular to the axis of rotation. The ratio of the length of the annulus to the gap width was $\Gamma=47.8$.

The inner cylinder, which was turned on a lathe to assure concentricity with the rotational axis, was driven by a stepper motor capable of microstepping at 25 000 steps per revolution. An optical encoder with a resolution of 300 pulses per

revolution was used for computer control of the rotational speed of the inner cylinder to better than 0.1% for the range of speeds used in these experiments.

The working fluid was a glycerol–water mixture with silver-coated hollow glass spheres (Potters Industries, NJ) added as PIV seed particles in a volume concentration of about 1.0×10^{-4} . The particles had a density of 1.6 g/cm^3 and an average diameter of $14 \text{ }\mu\text{m}$. The particles remained in uniform suspension for several hours even with no flow because of their small size. The temperature of the working fluid, which was room temperature, varied by no more than $0.5 \text{ }^\circ\text{C}$ over the course of a 1–1.5 h experiment. The viscosity of the working fluid, which was based on the average temperature during an experiment, was between 3.0 and 3.3 cSt, measured using a falling ball viscometer with an uncertainty of less than 1%.

The uncertainty in the Reynolds number due to the variation in the inner cylinder speed, fluid viscosity, and other factors was at most 4%. The uncertainty in the velocity measurements depends on the ability of seed particles to follow the flow and the accurate measurement of the particles' average displacement between PIV images. The seed particles were assumed to follow the flow quite accurately because the Stokes number was several orders of magnitude less than 0.14, the maximum Stokes number for which a particle can be assumed to accurately follow the flow.³¹ A cross-correlation PIV algorithm with a Gaussian fit for the correlation peak³² provided subpixel resolution to determine particles' average displacement between images across a grid of small interrogation regions in the illuminated plane. The temporal resolution in the delay between laser pulses of a few nanoseconds over a period of 1.2–5 ms resulted in negligible error.

For each Reynolds number at which velocity measurements were made, the annulus was filled with fluid, and the inner cylinder was run at high speed for a few minutes to thoroughly mix the fluid and the tracer particles. The inner cylinder was stopped and the working fluid was allowed to settle to quiescence with the particles remaining in suspension. Then the inner cylinder speed was quasistatically ramped to the desired speed at a relatively slow rate of 0.3 Re/s to avoid sensitivity of the system to the acceleration condition. After the inner cylinder reached the desired speed, the flow was allowed to develop at that Reynolds number for at least 10 min to ensure that the flow was fully developed before measurements began. Holding the inner cylinder speed constant and repeating the measurements some time later showed that this procedure generated repeatable results.

The flow velocities were measured using a TSI, Inc. Particle Image Velocimetry system based on cross-correlating a pair of images to avoid directional ambiguity. A dual Nd:YAG laser system was used to illuminate a horizontal plane through the vertical axis of the cylindrical Couette flow device. The laser sheet had a thickness of 1.0 mm. A TSI, Inc. Cross-Correlation CCD camera with resolution of 1000 by 1016 pixels was positioned to view the illuminated plane through a clear window in the end cap of the Couette cell. Each pixel in the image corresponded to $11.3 \text{ }\mu\text{m}$ in the flow field. The camera was fitted with a telecentric lens to avoid

parallax viewing along the narrow annulus that otherwise made it quite difficult to determine the exact position of the sidewalls. Because of the limited focal length of the telecentric lens, the illuminated measurement plane was about one-quarter of the annulus length from the window in the end cap. Velocity vectors were calculated on a rectangular grid of 15 points in the direction tangent to the circumference of the inner cylinder and 21 points perpendicular to the tangent direction. Based on comparing PIV results with the analytic solution for nonvortical flow, interrogation regions of 128 by 64 pixels with 50% overlap provided optimal results. Typically, 150 image pairs were acquired at either 5 or 15 Hz, corresponding to the passage of 7 to 8 azimuthal waves. The time between laser pulses in each pair ranged from 0.0012 to 0.005 s, depending on the Reynolds number to assure a particle displacement of 13–15 pixels between images in the fastest part of the flow field. The velocity vectors calculated on the rectangular grid were later interpolated onto a polar grid concentric with the cylinders. PIV measurements of stable circular Couette flow ensured that the PIV system correctly measured the azimuthal velocity within 1% and the radial velocity to within 4% of the inner cylinder speed.

PIV measurements were made at 16–18 latitudinal planes (perpendicular to the axis of rotation). The measurement planes were spaced by 1.78 mm ($\Delta z \sim 0.18d$). Thus, measurements were made over an axial extent of about $3d$ to assure capturing at least two full vortices. The lowest measurement plane was 10.8 cm from the lower endwall of the Couette cell to accommodate the focal length of the telecentric lens and to permit a clear image of the measurement plane through the necessary depth of seeded fluid. This position is about $11d$ from the endwall, far enough to avoid any undesirable effects related to Ekman vortices at the endwalls.

The critical Reynolds number at the onset of Taylor vortex flow for $\eta = 0.81$ is $\text{Re}_c = 97.1$, based on interpolation of a theoretical prediction.³³ Nonwavy Taylor vortex flow in the test cell was characterized by 24 pairs of vortices in the annulus. Wavy vortices were first easily detectable using PIV at $\text{Re} = 126$, or at a reduced Reynolds number of $\varepsilon = \text{Re}/\text{Re}_c - 1 = 0.28$, consistent with previous results that indicate the transition to wavy flow occurs for $0.09 \leq \varepsilon \leq 0.31$ for $0.8 \leq \eta \leq 0.9$.^{9,12,14,34,35}

III. WAVY VORTEX FLOW

A. Constructing the three-dimensional experimental velocity field for wavy vortex flow

Wavy vortex flow is a very complex flow to measure and analyze because it is unsteady and fully three-dimensional (three components of velocity and three nonzero gradients of velocity), compared with nonwavy Taylor vortex flow, which is steady and has no azimuthal gradient ($\partial_\theta = 0$). Thus, reconstructing the complete velocity field from PIV measurements in azimuthal and latitudinal planes was challenging and somewhat complicated.

To begin, it was necessary to reconstruct an entire azimuthal wave from many short segments of the wave obtained in several latitudinal ($r-\theta$) planes. The difficulty resulted from the PIV image area extending only about 12°

around the annulus, only 13% of the azimuthal wavelength for the condition of four waves around the annulus. Multiple overlapping PIV image pairs were obtained in each latitudinal plane. Knowing the wave speed, the image pairs could be pieced together to provide the composite velocity field for an entire wave. (An analogy would be taking many pictures of a train as it passed by a camera at a fixed location. By placing individual pictures of short sections of the train side-by-side, a composite picture of the entire train could be created.) PIV images were recorded long enough to include about 7.6 waves, owing to limitations in computer storage of the image files. Based on the wave speed, the records at equivalent phases in the wave were ensemble averaged. Then the radial velocity profile was smoothed by Fourier transforming the data, eliminating the highest frequency components, and then inverse Fourier transforming the data back into the time domain. This created a typical radial-azimuthal ($v_r - v_\theta$) velocity field for that $r-\theta$ plane. The process was repeated at about 18 axial locations to provide measurements in latitudinal planes spanning more than two vortices.

Since the measurements in each latitudinal plane were obtained independently, it was necessary to phase-align the measurements with one another. Our previous measurements of wavy vortex flow in a meridional plane indicate that there is no phase difference for different parts of the wavy vortex.¹¹ In other words, the axial motion of the inflow boundary, the outflow boundary, and the vortex center in the velocity field are in phase with each other as a wavy vortex passes through a meridional plane. This permitted the relative rotation of velocity measurements in a particular latitudinal plane with respect to another latitudinal plane by matching the minima and maxima of the radial velocity field in the two planes. This was repeated for all latitudinal planes so the extrema in the radial velocity in all of the $r-\theta$ planes were aligned to obtain a complete phase-matched radial-azimuthal velocity field. Approximately 12 latitudinal planes correspond to the axial extent of a vortex pair, although the matching was based on 16 latitudinal planes to assure that the entire vortex pair was captured.

The entire three-dimensional velocity field was constructed by combining the current measurements in latitudinal ($r-\theta$) planes with previous measurements in meridional ($r-z$) planes,¹¹ shown schematically in Fig. 1, using the radial velocity, which was measured in both cases. Before this could be accomplished, it was necessary to interpolate the velocities onto comparable grids, since the numbers of vectors calculated across the annular gap was different for the latitudinal and meridional planes. In addition, the velocity was measured at only 8 meridional planes for each wave, while it was measured at much higher resolution in the latitudinal plane measurements. This, however, was not without complications. Although the apparatus was nearly the same for measurements in the latitudinal planes and the meridional planes, the inner and outer cylinders were slightly different owing to the need to avoid reflections of the laser light from the cylinders in slightly different ways for the measurements in the different planes. Consequently, the radius ratio for the latitudinal measurements was $\eta=0.81$, while it was $\eta=0.83$ for the meridional plane measurements. This minor

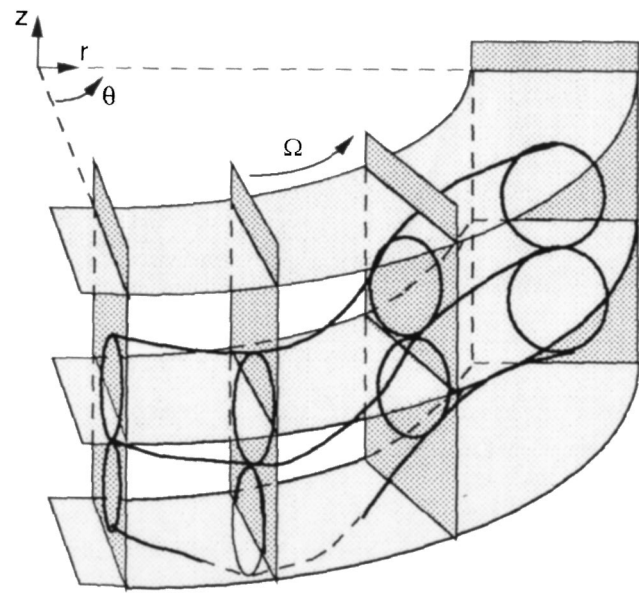


FIG. 1. Schematic of the meridional and latitudinal measurement planes. The latitudinal ($r-\theta$) planes were shifted azimuthally and axially as a group with respect to the meridional ($r-z$) planes to minimize the rms difference in the radial velocity, which was measured in both cases, resulting in the complete three-dimensional velocity field.

difference has a slight effect on the theoretical critical Reynolds number [$Re_c=97$ for $\eta=0.81$ vs $Re_c=102$ for $\eta=0.83$].³³ As a result, two corrections were necessary. First, the rotational speeds in the current measurements were adjusted so that the reduced Reynolds number, ε , matched that in the meridional plane experiments. Second, all distances were scaled based on the gap width before aligning the velocity fields.

The final interpolation grid consisted of 90 points in the azimuthal direction for one wave at $\varepsilon=1.48, 5.03$ (4 azimuthal waves around the annulus) and 180 points for one wave at $\varepsilon=0.28$ (2 azimuthal waves around the annulus), 19 points between the inner and outer cylinder (plus the boundary conditions on the inner and outer cylinders), and 24 points axially extending two vortices (32 points for $\varepsilon=5.03$). The resulting interpolated grid spacing is indicated in Table I. The exact value for the axial wavelength λ listed in Table I was somewhat problematic to determine, since it is based on measurements in a finite number of latitudinal planes, thereby limiting the axial resolution. In addition, it required matching velocity fields at two slightly different radius ratios. The wavelength indicated in Table I is the average value over several waves with a confidence of $\pm 1\%$. The wavelengths are similar to those for previous experiments and theory.^{36,37}

TABLE I. Wavelength and resolution of interpolated velocity field.

ε	λ/d	$\Delta r/d$	$\Delta \theta$	$\Delta z/d$
0.28	2.16	0.050	1°	0.090
1.48	2.16	0.050	1°	0.090
5.03	2.18	0.050	1°	0.068

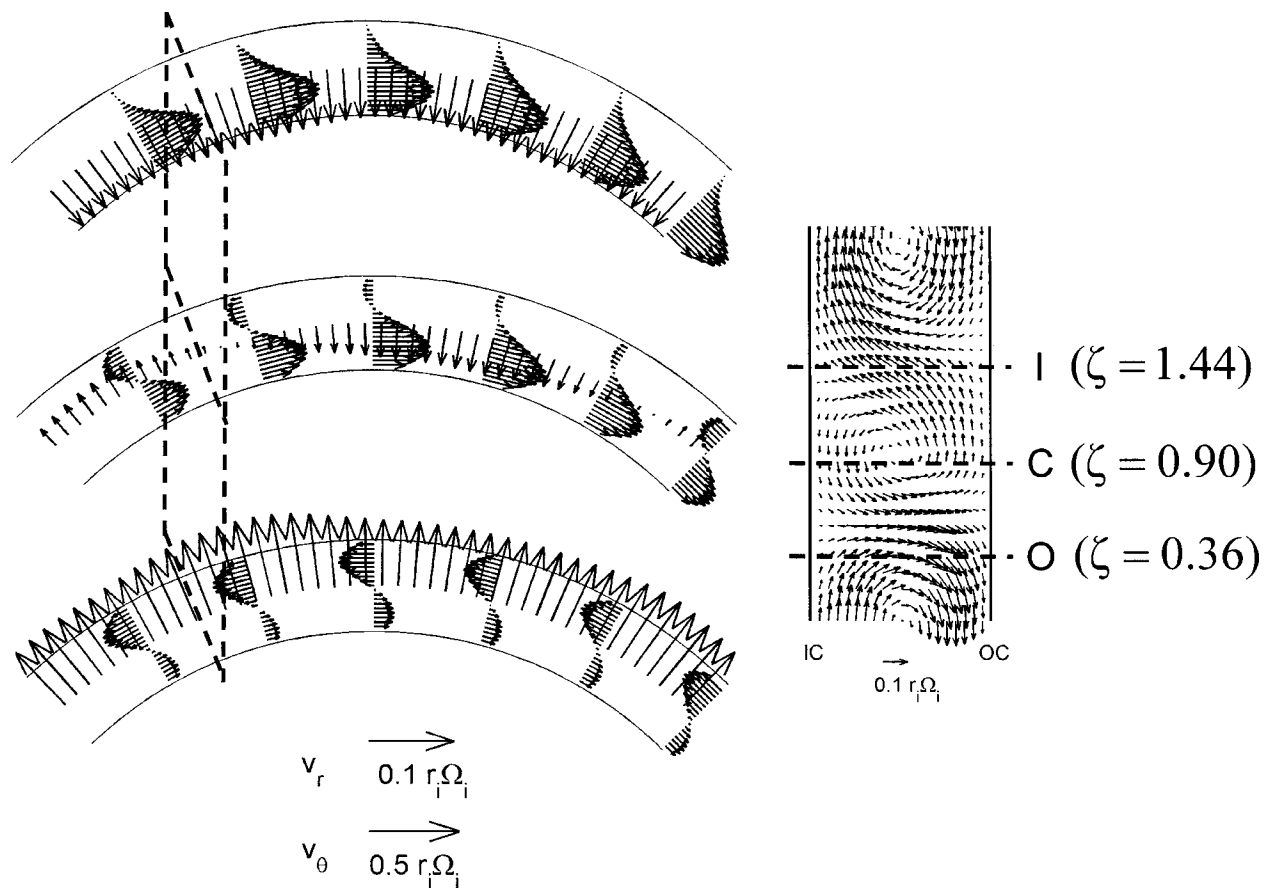


FIG. 2. Radial velocity (v_r) and azimuthal difference velocity ($v_\theta - v_{\theta,stable}$) in a latitudinal plane shown at inflow (top), vortex center (middle), and outflow (bottom) boundaries for $\varepsilon = 1.48$. The dashed lines represent the azimuthal position of the meridional plane that is shown on the right. The dashed lines shown on the meridional plane represent the axial position of the latitudinal planes. The inner cylinder rotates counterclockwise.

After the interpolation, the data set was smoothed by removing high wavenumber components in the Fourier transform of the velocity profiles that were related to experimental noise. At this point, the radial velocities could be matched between the meridional plane measurements and the latitudinal plane measurements, shown schematically in Fig. 1. This required rotating the latitudinal planes as a group and shifting them axially as a group with respect to the meridional planes until the rms difference between the two radial velocities was minimized. Thus, using the azimuthal and axial periodicity in the velocity field permitted the construction of the complete three-dimensional velocity field for all three velocity components for a single azimuthal wave and extending axially slightly more than one axial wavelength. This process was repeated for the three rotational speeds corresponding to $\varepsilon = 0.28, 1.48, \text{ and } 5.03$.

An example of the velocity field is shown in Fig. 2 for $\varepsilon = 1.48$. The radial and axial velocities are shown in the meridional plane. The difference between the measured azimuthal velocity (v_θ) and the theoretical azimuthal velocity for the stable cylindrical Couette flow ($v_{\theta,stable}$) at the same Reynolds number is used here for the azimuthal velocity to more readily display the details of the azimuthal velocity field. Using $(v_\theta - v_{\theta,stable})/r_i\Omega_i$ for the azimuthal velocity amplifies the deviation of the velocity profile from that for

nonvortical flow that results from the transport of azimuthal momentum by the Taylor vortices.

At this Reynolds number the flow has four azimuthal waves, so one-quarter of the annulus depicts one wavelength. Each of the quarter-circle sections on the left-hand side of the figure shows the azimuthal velocity at six positions along the wave and the radial velocity at the middle of the annular gap. The upper curve is the outer cylinder, and the lower curve is the inner cylinder, which is rotating counterclockwise. The three quarter-circle sections are at the latitudinal planes $\zeta = z/d = 0.36, 0.90, \text{ and } 1.44$, corresponding approximately to an inflow region between vortices (I), the center of the vortex (C), and an outflow region between vortices (O). The axial position $z=0$ was arbitrarily set at the bottom of the meridional measurement plane, which is shown on the right-hand side of Fig. 2, and is located approximately $11d$ from the bottom of the annulus. The left boundary of the meridional plane is the rotating inner cylinder (IC) and the right-hand side is the stationary outer cylinder (OC). The meridional plane intersects the latitudinal planes near the left end of the latitudinal sections as indicated by the dashed lines. Likewise, the positions of the latitudinal planes are indicated by dashed lines on the meridional plane labeled I, C, and O. The middle latitudinal plane is near the center of the vortex where the downward axial

flow occurs near the inner cylinder and upward axial flow occurs near the outer cylinder. Of course, the radial velocity varies with axial position, depending on what portion of the vortex is sliced by the latitudinal plane. In the upper latitudinal plane in Fig. 2, which is above the vortex center, the flow is radially inward. The lower plane in Fig. 2 is below the vortex center where the flow is outward. In these regions, the radial velocity is nearly uniform with θ , but it varies substantially with θ at the center of a vortex. The radial velocity in the middle latitudinal plane is zero at two points, corresponding to the curve coincident with the center of the vortex, which necessarily pierces the latitudinal plane twice.

Of course, the variation in the radial velocity with θ results in a variation in the azimuthal velocity with θ . The scale for the azimuthal velocity difference vectors ($v_\theta - v_{\theta, \text{stable}}$), which is displayed at the bottom of Fig. 2, is more than 5 times that for the radial velocity (v_r) reflecting the order of magnitude difference in these velocities. The inner cylinder is moving to the left in the latitudinal planes shown in this paper. An azimuthal velocity difference ($v_\theta - v_{\theta, \text{stable}}$) to the left indicates that fluid is locally moving faster than it would if the flow were nonvortical (a velocity surplus); an azimuthal velocity difference to the right indicates fluid moving slower than stable flow (a velocity deficit). Of course, at the walls of the annulus, the velocity difference is zero. Nevertheless, for some of the azimuthal velocity profiles shown in Fig. 2, visual inspection suggest that the profiles may not go to zero, particularly at the inner wall. The problem is complicated by the inability of PIV to measure extremely close to a wall, because the PIV interrogation region overlaps the wall. However, careful inspection of the velocity data revealed that the velocity gradient near the wall is quite steep. Simply extrapolating the velocity profile by eye does not accurately account for the steep velocity gradient at the wall.

In the inflow region in the upper latitudinal plane, the radially inward velocity carries low azimuthal momentum from the outer fixed cylinder inward decreasing the azimuthal velocity across the entire annulus compared to what it would be for nonvortical flow. On the other hand, the radially outward velocity in the lower latitudinal plane carries high azimuthal momentum outward from the inner rotating cylinder resulting in substantial velocity surplus near the outer cylinder. However, an azimuthal velocity deficit occurs in outflow regions near the inner cylinder as low momentum fluid is carried upward along the inner cylinder. Near the center of the vortex, corresponding to the middle latitudinal plane in Fig. 2, the azimuthal velocity surplus or deficit depends on the rotation of the vortex and the fluid that is carried with it. In this case, the vortex is rotating so that the flow is downward at the inner cylinder carrying low momentum fluid from the inflow boundary with it across the plane near the center of the vortex. The result is a velocity deficit near the inner cylinder. The upward flow near the outer cylinder carries higher momentum fluid from the outflow boundary with it augmenting the azimuthal velocity at the outer cylinder. Of course, the opposite situation occurs in the adjacent vortex (not shown) because the vortex rotates with the opposite sense.

B. 3-D experimental velocity field for wavy vortex flow

Now it is possible to consider the velocity field in the latitudinal plane for several slices spanning a vortex pair, as shown in Fig. 3 for $\varepsilon = 1.48$. The slices through a vortex pair are shown starting from the top of a vortex pair in the upper left to the bottom of the vortex pair in the lower right. The velocity field in the highest latitudinal plane ($\zeta = 2.34$ in the upper left) is near an outflow region. Moving downward in the left column the planes pass through a vortex center and then an inflow region. Moving top to bottom in the right column the planes begin near an inflow region, pass through another vortex center, and finally to another outflow region ($\zeta = 0.36$). The next slice below that in the lower right corner is periodic with the slice shown in the upper left corner.

The radial velocity varies substantially with axial and azimuthal position. The azimuthal velocity profile is fairly uniform with θ at the inflow region ($\zeta = 1.44$) and the outflow region ($\zeta = 0.36$). Upon close examination, it is evident that the outflow is stronger than the inflow, consistent with previous measurements in nonwavy and wavy Taylor vortex flow.^{6-9,38} At other axial positions, the radial velocity varies substantially due to the waviness of the vortices. Positions of zero radial velocity in some latitudinal planes correspond to the center of the vortex.

The effect of the radial velocity on the azimuthal velocity profile ($v_\theta - v_{\theta, \text{stable}}$) is dramatic as the wavy vortical motion redistributes the azimuthal velocity to different degrees along the length of the wave. For axial positions where the radial velocity is relatively uniform, such as near the inflow boundary at $\zeta \sim 1.5$ or the outflow boundary at $\zeta \sim 0.5$, the azimuthal velocity profile varies only slightly with azimuthal position. At axial positions where the radial velocity changes sign, such as at the vortex centers ($\zeta \sim 0.9$ and 2.0), the azimuthal velocity profile varies substantially in a single latitudinal plane. Interestingly, the azimuthal velocity deficit for radial inflow is substantially greater than the velocity surplus for radial outflow. Furthermore, the velocity deficit for inflow extends across the entire annulus, whereas the velocity surplus at an outflow region only occurs near the outer cylinder. Similar results occur for all three Reynolds numbers that were measured. It has been shown both experimentally and computationally that, on average, the gradient near the outer cylinder is not as steep as that near the inner cylinder and that the deviation of the velocity profile from nonvortical is not as severe near the outer cylinder as near the inner cylinder.^{9,13} The implication is that the azimuthal velocity is augmented over less of the flow domain (only near the outer cylinder in outflow regions) than it is diminished (in the inflow region and near the inner cylinder in the outflow region). The result is the asymmetry in the azimuthal flow between the inflow and outflow regions.

Figure 4 shows contours of the out-of-plane axial component of velocity. The latitudinal planes shown in the figure correspond to those in Fig. 3. The asterisks mark where the curve coincident with the center of the wavy vortex passes through the latitudinal plane. Near the center of a vortex ($\zeta \sim 0.9$), the axial velocity is downward near the inner cylinder

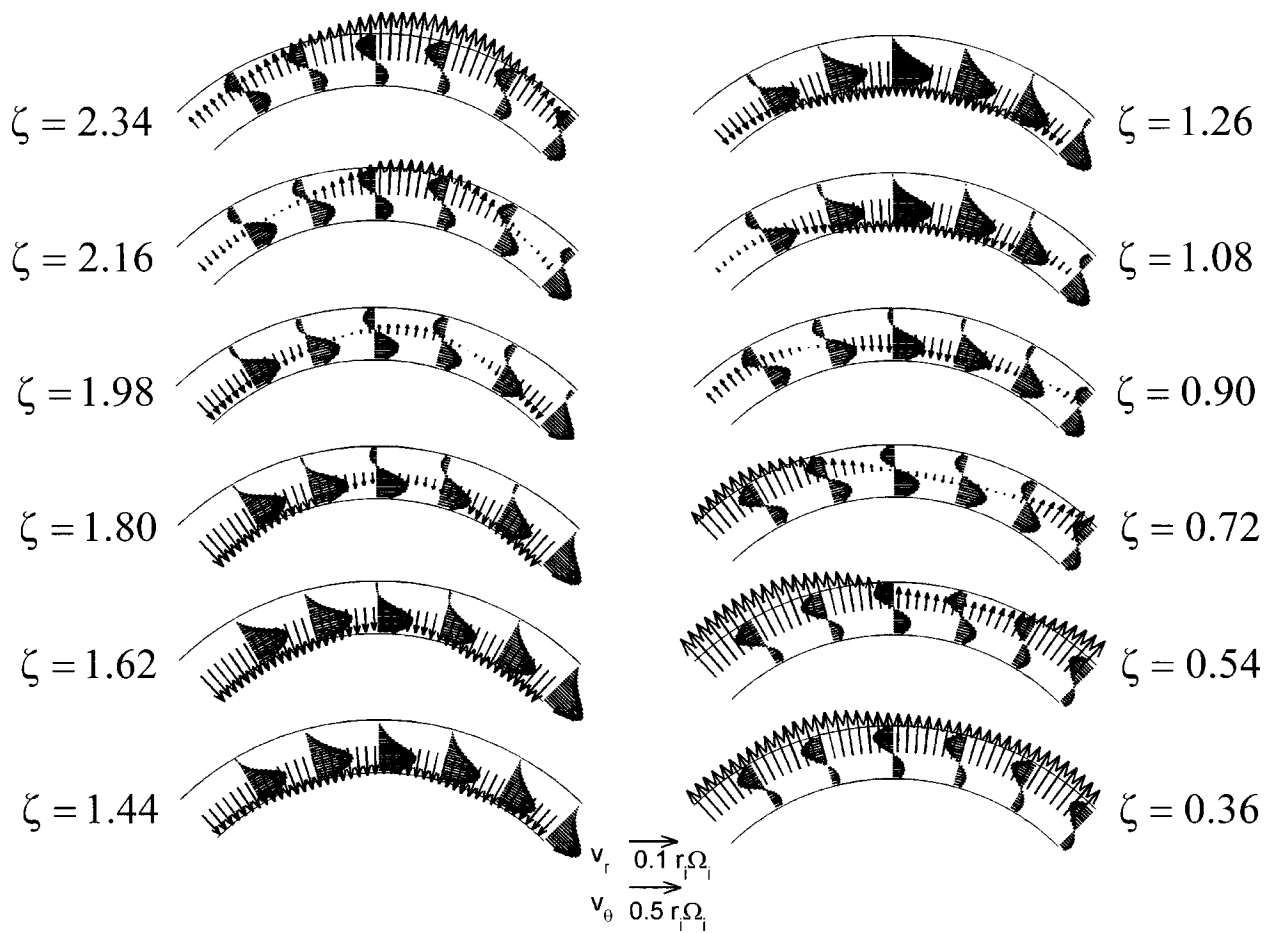


FIG. 3. Velocity field in the latitudinal plane for several latitudinal slices spanning a vortex pair in the axial direction for $\epsilon = 1.48$. The axial positions of the latitudinal planes have the same relationship to the wave as indicated in Fig. 2.

der and upward near the outer cylinder. At the center of the adjacent vortex ($\zeta \sim 2.0$), the axial velocity is opposite. However, at the inflow boundaries ($\zeta \sim 1.5$) or outflow boundaries ($\zeta \sim 0.5$), the positive and negative axial velocity contours extend across the gap. The axial velocities in these regions are less than those near the center of the vortex (based on the number of contours), but not substantially less.

These latitudinal planes can be imagined to be stacked one on top of the other with the shaded region corresponding to downward axial velocity greater than $0.06r_i\Omega$. A continuous region of downward axial velocity starts near the outer cylinder at $\zeta = 2.34$ and extends downward. From top to bottom (decreasing ζ) this region of negative axial velocity moves to the right and then crosses the annulus to the inner cylinder by $\zeta = 1.26$. It then moves left and back across the annulus to the outer cylinder to repeat the situation in the next vortex pair. A similar result occurs for positive axial velocity contours, although the region is not shaded in the figure. Of course, these regions of positive or negative contours correspond to continuous upward or downward streams of axial flow in the annulus extending the entire length of the annulus between vortices and across vortex pairs. They correspond to azimuthal locations where the velocity field in a meridional plane appears as shown at position I in Fig. 2, where there is an upward axial flow from one vortex to another. Although Wereley and Lueptow identified these re-

gions of net axial flow,¹¹ they were unable to detect that these axial flow streams wind from the inner cylinder to the outer cylinder and back as indicated in Fig. 4.

The results in Fig. 4 indicate that wavy vortex flow should be viewed quite differently from the simplistic ideal of independent, wavy, toroidal vortex tubes. Instead, fluid flows in continuous axial streams that extend axially through the entire stack of wavy vortices along the length of the annulus. These streams of upward and downward axial flow wind from side to side and from the inner to outer cylinder connecting adjacent vortices and permitting fluid to flow substantial axial distances when compared to the axial dimension of the vortex. An upward and a downward axial stream occur for each wave, so for the 4-wave system at $\epsilon = 1.48$ shown in Fig. 4, there are four upward streams and four downward streams in the annulus. Of course, this axial transport together with the azimuthal velocity leads to the enhanced chaotic mixing and transport in wavy vortex flow that has been studied in some detail.^{39–46}

Apart from the streams of axial flow, there seems to be no obvious relation between the radial and azimuthal velocity vectors in a latitudinal plane (Fig. 3) and the axial velocity contours (Fig. 4). It is, however, useful to note the positions where the three-dimensional contour of the vortex centers intersects the planes, marked with a pair of asterisks (for two intersections) in four of the planes shown in Fig. 4.

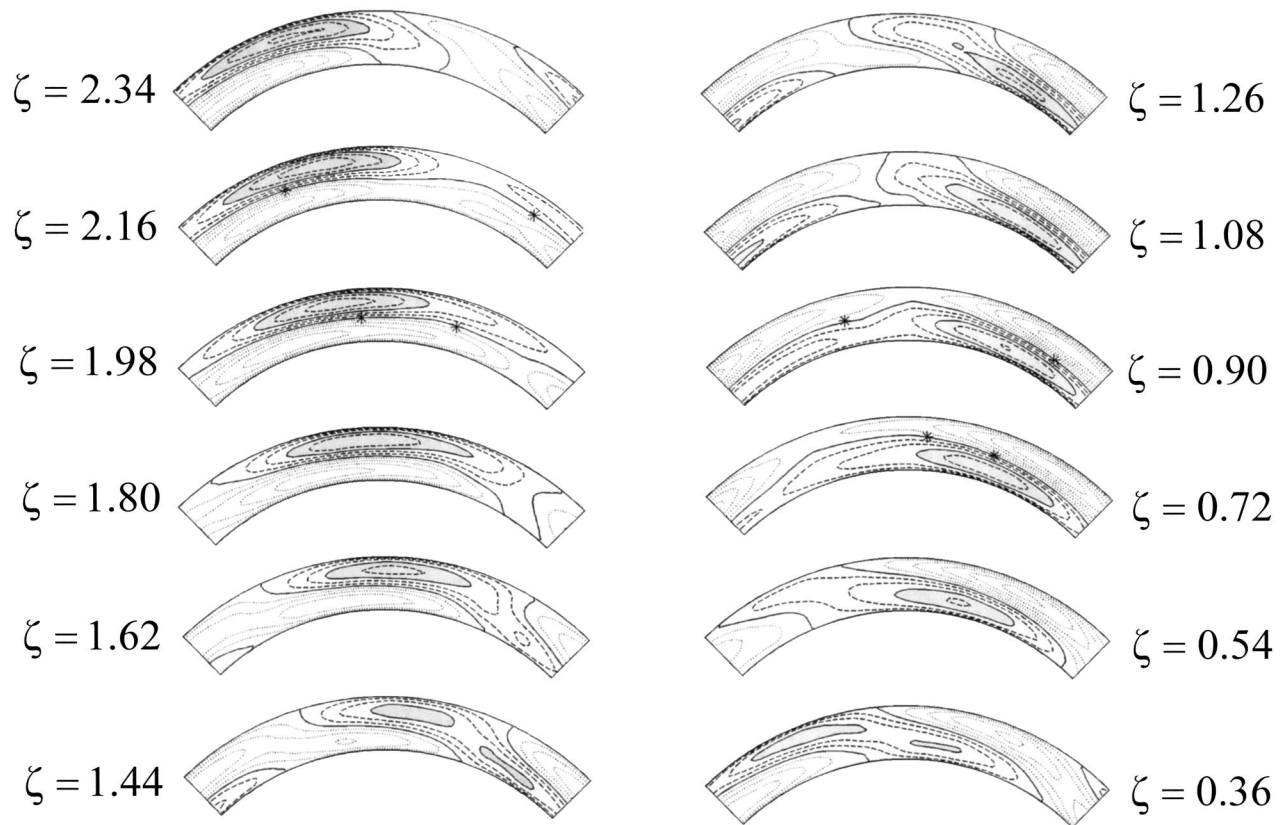


FIG. 4. Axial velocity contours in the latitudinal plane for several latitudinal slices spanning a vortex pair in the axial direction for $\varepsilon = 1.48$. The velocity increment between contour lines is $0.02r_i\Omega$. Positive contours are dotted; negative contours are dashed; contours for zero and $-0.06r_i\Omega$ are solid. In the shaded region, $v_z < -0.06r_i\Omega$. Asterisks denote the positions where the curve coincident with the center of the vortex intersects the latitudinal planes.

The intersection is, of course, always at the contour of zero axial velocity. It is interesting that the pair of intersections is not symmetric with respect to the high axial velocity regions (shaded contours), but is offset to one side.

Although the axial motion of wavy vortices is obvious from flow visualization, it has recently been shown that the vortex centers oscillate radially as well as axially.¹¹ A projection of the instantaneous radial position of the vortex center on a latitudinal plane is shown in Fig. 5. At $\varepsilon = 1.48$, which corresponds to the Reynolds number for the maximum radial displacement,¹¹ the solid curve indicating the amplitude of the vortex center motion is about 22% of the gap width. Hatched curves concentric with the cylinders in Fig. 5 indicate the minimum and maximum radial position for this case. At other Reynolds numbers the displacement of the vortex centers is less. For $\varepsilon = 0.28$ (dot-dash curve), the vortex cen-

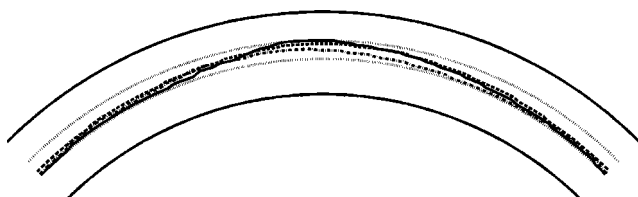


FIG. 5. Azimuthal position of vortex centers. Dotted-dashed curve is $\varepsilon = 0.28$; solid curve is $\varepsilon = 1.48$; dashed curve is $\varepsilon = 5.03$; dotted curves are the maximum and minimum limits of radial vortex motion at $\varepsilon = 1.48$.

ter moves across 10% of the gap and for $\varepsilon = 5.03$ (dashed curve), the vortex center moves across 12% of the gap. (In the case of $\varepsilon = 0.28$, the path of the vortex center is compressed from π [2 waves around the annulus] to $\pi/2$ to show the entire path in the same figure as the other Reynolds numbers.)

The three components of the velocity field can be shown simultaneously in meridional planes. Figure 6 depicts the radial and axial velocities as vectors and the out-of-plane azimuthal velocity as contours for four phases in a wave at $\varepsilon = 1.48$. The sequence can be thought of as four meridional slices through a single wave at equally spaced azimuthal positions or as snapshots of the flow at four instants in time as a wave passes through a single meridional plane. As described by Wereley and Lueptow,¹¹ there is significant axial, inter-vortex flow that changes depending on the phase in the cycle. At the first instant shown, there is a net upward flow winding around the vortices, while at the third instant shown, there is a net downward flow. At the second instant, there is a downward axial flow between the vortices so that the lower vortex has fluid flowing into it, while at the fourth instant, the same vortex has fluid flow out of it.

The contours of the azimuthal velocity in Fig. 6 show the impact of the inter-vortex flow and vortical flow on the azimuthal velocity. Near vortex centers the azimuthal velocity contours are oriented radially indicating a uniform azimuthal velocity across a significant portion of the annular

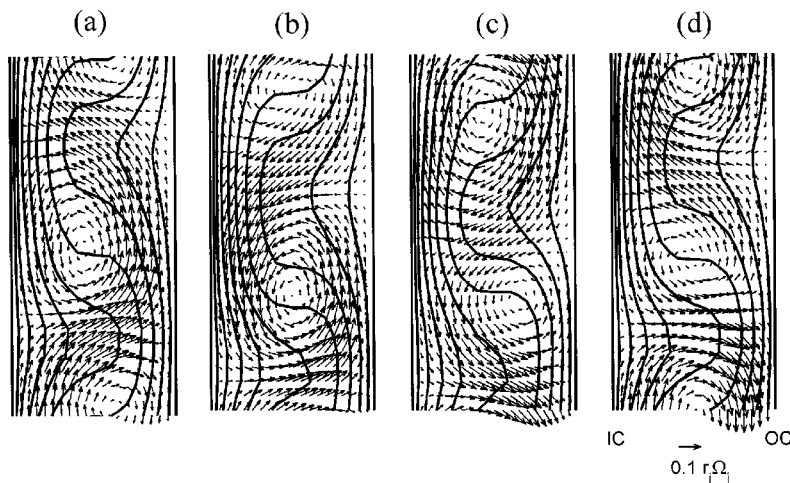


FIG. 6. Radial (v_r) and axial (v_z) velocity vectors in a meridional plane overlaid with azimuthal velocity (v_θ) contours shown at equally spaced azimuthal positions for $\varepsilon = 1.48$. (a) $r\theta = 0$, (b) $r\theta = \lambda/4$, (c) $r\theta = \lambda/2$, and (d) $r\theta = 3\lambda/4$, where λ is the azimuthal wavelength, which corresponds to an angle of $\pi/2$ for four azimuthal waves. The azimuthal velocity contours are equally spaced between 0 at the outer cylinder (OC) and $1.0r_i\Omega$ at the inner cylinder (IC).

gap. In inflow regions, the contours are quite close to each other near the inner cylinder resulting in locally high shear stress while the contours are spaced quite far apart near the outer cylinder. The converse does not occur to the same extent in outflow regions. Instead, the contours in an outflow region remain closely spaced near the walls of both cylinders while becoming widely spaced at the center of the annular gap. The result is an axially and azimuthally varying shear stress at the outer cylinder while the shear stress is much more uniform at the inner cylinder. The vortex centers remain at positions corresponding to nearly the same azimuthal velocity at all phases in the wave, even though the position of the vortex center moves both radially and axially. The vortex center is at a position corresponding to an azimuthal velocity that is about 40% that of the inner cylinder. This result is quite interesting in that the wave speed of the traveling azimuthal wave for these experiments is about $0.4r_i\Omega$ at this Reynolds number.¹¹ The similarity in the azimuthal velocity at the center of a vortex and the wave speed suggests that while fluid near the inner cylinder travels much faster and fluid near the outer cylinder travels much slower, the structure to which the wave speed corresponds travels with the vortex center. This result has implications for the origin of the azimuthal waviness as discussed shortly.

The effect of the Reynolds number on the velocity field is shown in Fig. 7. At low Reynolds numbers, the vortical motion is much weaker than at higher Reynolds numbers. The length of the velocity vectors indicates that the radial and axial velocities at low Reynolds numbers are a smaller proportion of the surface speed of the inner cylinder than at higher Reynolds numbers. Of course, the absolute (non-scaled) magnitude of the vortical velocity increases substantially with Reynolds number as well. The strength of the vortices affects the degree of distortion of the azimuthal velocity contours. At the lowest Reynolds number, the contours are smoothly distorted by the vortical flow. At higher Reynolds numbers the distortion is significant. In fact, at $\varepsilon = 5.03$ the vortical flow is strong enough to wrap the azimuthal velocity contours around the vortex centers slightly and create relative large regions across the annular gap where the azimuthal velocity does not vary substantially. Note that the position of the vortex center corresponds to

decreasing azimuthal velocity contours as the Reynolds number increases: about $0.45r_i\Omega$ at $\varepsilon = 0.28$ to about $0.35r_i\Omega$ at $\varepsilon = 5.03$. This decrease in azimuthal velocity is similar to the decrease in azimuthal wave speed with increasing Reynolds number,^{11,47} further suggesting a relation between the azimuthal velocity of the fluid near the vortex center and the azimuthal wave speed.

The distortion of the azimuthal velocity contours is directly dependent on the phase of the wave. Figure 8 shows the azimuthal velocity contour, $v_\theta/r_i\Omega$, that corresponds to the wave speed, $v_{\text{wave}}/r_i\Omega$, throughout one wave at $\varepsilon = 1.48$. In other words, the fluid at each contour is moving at precisely the same speed as the azimuthal wave. Figure 8(a) shows five contours uniformly sampled in time through the first half of the wave; Fig. 8(b) shows the second half of the wave. If the contours were animated, they would move according to the arrows as time progresses. The bold contours, which are identical in Figs. 8(a) and 8(b), indicate the beginning and end of the half-phase. The bulges in the contours

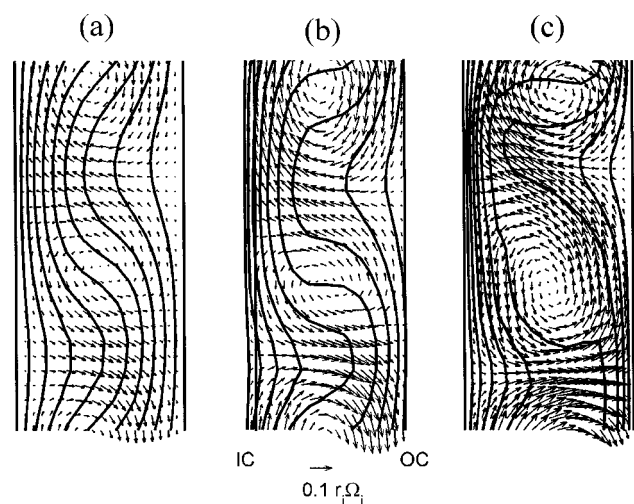


FIG. 7. Radial (v_r) and axial (v_z) velocity vectors in a meridional plane overlaid with azimuthal velocity (v_θ) contours shown at the same approximate phase of the azimuthal wave. (a) $\varepsilon = 0.28$, (b) $\varepsilon = 1.48$, (c) $\varepsilon = 5.03$. The azimuthal velocity contours are equally spaced between 0 at the outer cylinder (OC) and $1.0r_i\Omega$ at the inner cylinder (IC).

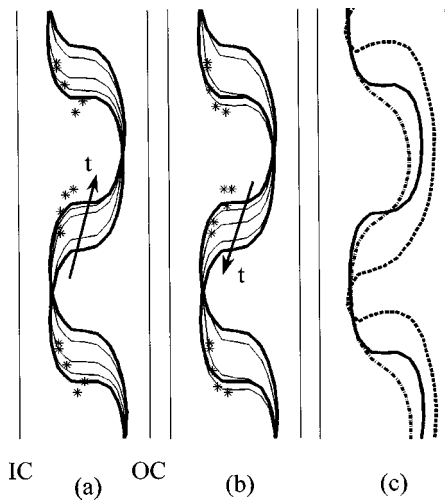


FIG. 8. Azimuthal velocity (v_0) contour corresponding to the wave speed at $\epsilon = 1.48$: (a) up-cycle; (b) down-cycle. The limit contours at each half-cycle are bold; (*) vortex centers. (c) Contours corresponding to the wave speed at approximately the same phase of the wave for $\epsilon = 0.28$ (dash-dot), $\epsilon = 1.48$ (solid), and $\epsilon = 5.03$ (dashed).

result from the radial transport of azimuthal momentum by the vortices: inflow regions correspond to leftward maxima in the contours while outflow regions correspond to rightward maxima in the contours. An animation of these figures indicates that not only do the bulges oscillate up and down with the azimuthal wave, they subtly change in axial extent. These changes are not sinusoidal. At certain points in the phase, the axial extent of the bulges changes more quickly than at other points in the phase. The asterisks in Fig. 8 indicate the instantaneous position of the vortex center, which moves radially as well as axially, even though the wave speed contour remains essentially centered in the annulus. The vortex center remains fairly close to the wave speed contour, but is in the region of fluid that is just slightly faster than the wave speed.

The character of these contours changes substantially with the Reynolds number as indicated in Fig. 8(c). At the lower two Reynolds numbers (dash-dot and solid curves), the leftward (inflow) and rightward (outflow) bulges are similar in size. The outflow is much stronger at the higher Reynolds number (dashed curve) resulting in a broadening of the outflow bulge and a narrowing of the inflow bulge. In this case, the inflow bulge is only about one-third as wide as the outflow bulge. The strength of the outflow also results in this contour shifting radially outward. The fluid to the left of the contour is moving faster than the wave speed, while the fluid to the right is moving more slowly. At the highest Reynolds number, a very large proportion of the fluid moves faster than the wave speed. At the lower Reynolds numbers about half the fluid moves faster than the wave speed and half moves slower. The axial transport between vortices is also evident in the contour at the highest Reynolds number. The narrow bulge to the left is tilted downward because of the net downward axial flow at this point in the phase.

In Fig. 9 the azimuthal velocity vectors are shown in a frame rotating with the speed of the traveling wave, which is equivalent to $(v_\theta - v_{\text{wave}})/r_i\Omega$, in a cylindrical surface con-

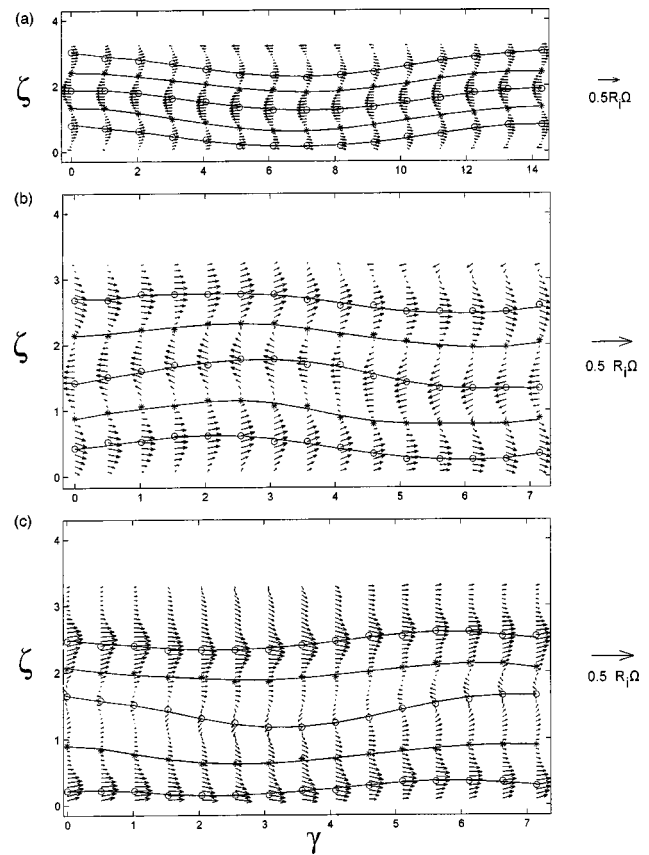


FIG. 9. Azimuthal velocity (v_0) in a frame rotating with the speed of the traveling wave in a cylindrical surface at a radial position midway across the annular gap. (a) $\epsilon = 0.28$, (b) $\epsilon = 1.48$, (c) $\epsilon = 5.03$. (*) Vortex centers; (O) outflow or inflow boundaries. Solid curves are least-squares fits.

centric with the axis of rotation at a position midway across the gap. The coordinate $\gamma = [(r_i + r_o)/2]\theta/d$ is the azimuthal distance along the cylindrical surface, so that $0 \leq \gamma \leq 7.42$ corresponds to one-quarter of the annulus. The asterisks correspond to the projections of the positions of the vortex centers, while the open circles correspond to inflow or outflow regions (based on the radial velocity). Curves are least squares fits through these positions. The traveling wave is moving to the right. Consequently, the inflow region has a velocity deficit with respect to the traveling wave speed (leftward vectors) and the outflow region has an augmented velocity (rightward vectors). The character of the azimuthal velocity changes substantially as the Reynolds number increases. At $\epsilon = 0.28$ and 1.48 , the contour of vortex centers corresponds fairly closely to the position of zero azimuthal velocity in the rotating frame. This means that the vortex center, which is near the middle of the annular gap, is traveling azimuthally at about the same velocity as the azimuthal wave. However, at the highest Reynolds number, $\epsilon = 5.03$, the azimuthal velocity is positive along the contour of vortex centers. This comes about because the azimuthal velocity is higher than the wave speed through a larger portion of the annular gap, as was evident in Fig. 8(c). Thus, the azimuthal velocity at the center of the annular gap is greater than the wave speed. The axial component of velocity is greatest for

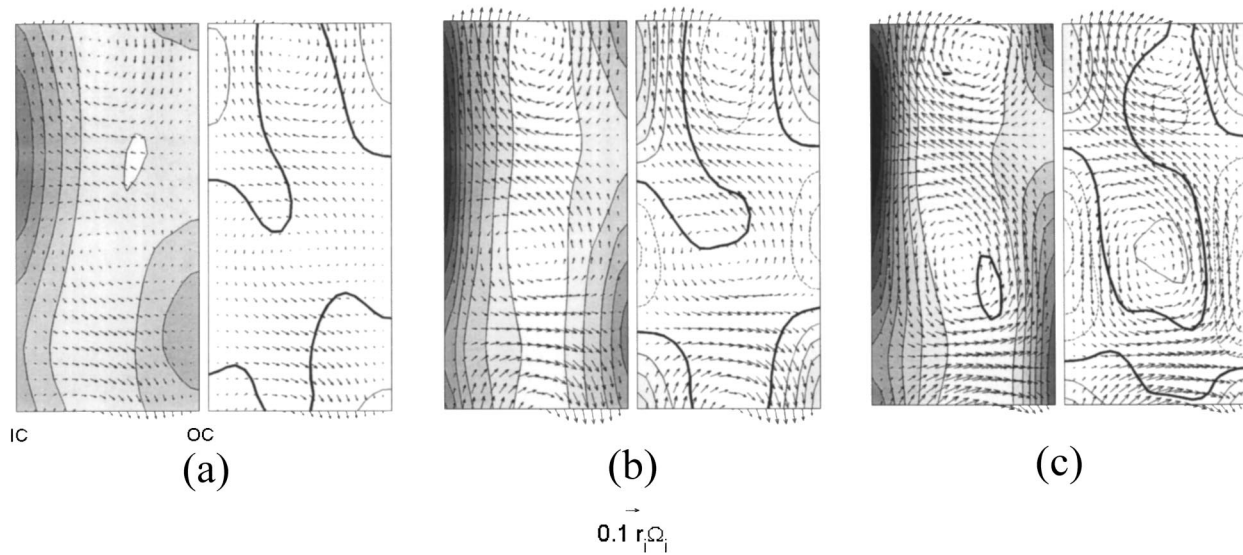


FIG. 10. Shear stress in a meridional plane overlaid with radial (v_r) and axial (v_z) vectors. (a) $\varepsilon=0.28$, (b) $\varepsilon=1.48$, (c) $\varepsilon=5.03$. In each part, the left plane is the azimuthal shear stress, $\tau_{r\theta}d/\mu r_i\Omega$, and the right plane is the axial shear stress, $\tau_{rz}d/\mu r_i\Omega$. Bold solid contours are zero shear stress. Solid contours are positive and dashed contours are negative shear stress. The contour spacing is 0.5 for azimuthal shear stress ($\tau_{r\theta}$) and 0.2 for axial shear stress (τ_{rz}).

$\varepsilon=1.48$, as first noted by Wereley and Lueptow.¹¹ It is also clear that the axial component of velocity is typically in the same direction as the wave amplitude. The flattening of the waviness at vortex centers and outflow boundaries compared to inflow boundaries is evident at the highest Reynolds number, consistent with previous results.¹¹

We can now turn to the question of the origin of the azimuthal waviness. Two shear layers in the azimuthal velocity are most clearly evident in Figs. 9(a) and 9(b) for the lower Reynolds numbers, although two shear layers also appear in Fig. 9(c) for the highest Reynolds number. Further note that at the two lower Reynolds numbers, the inflection in the azimuthal velocity occurs at the vortex center, which happens to be where the azimuthal velocity matches the

wave speed. Finally, the change in the azimuthal velocity from an inflow region to an outflow region is about $0.3 r_i\Omega$ (based on Fig. 9), whereas the change in the radial velocity across the same distance is less than half as much (based on Figs. 6 and 7). These results suggest that the azimuthal waviness is more likely related to an instability in the azimuthal velocity profile as the vortices redistribute the flow into streams of high and low azimuthal momentum, as suggested by Jones,¹⁴ than to the radial outflow jets.

From the velocity field it is possible to calculate the components of the shear stress using finite differences (central differences for the interior and forward/backward differences at the wall). Here we consider only $\tau_{r\theta}$ and τ_{rz} because they are important in determining the torque for inner cylin-

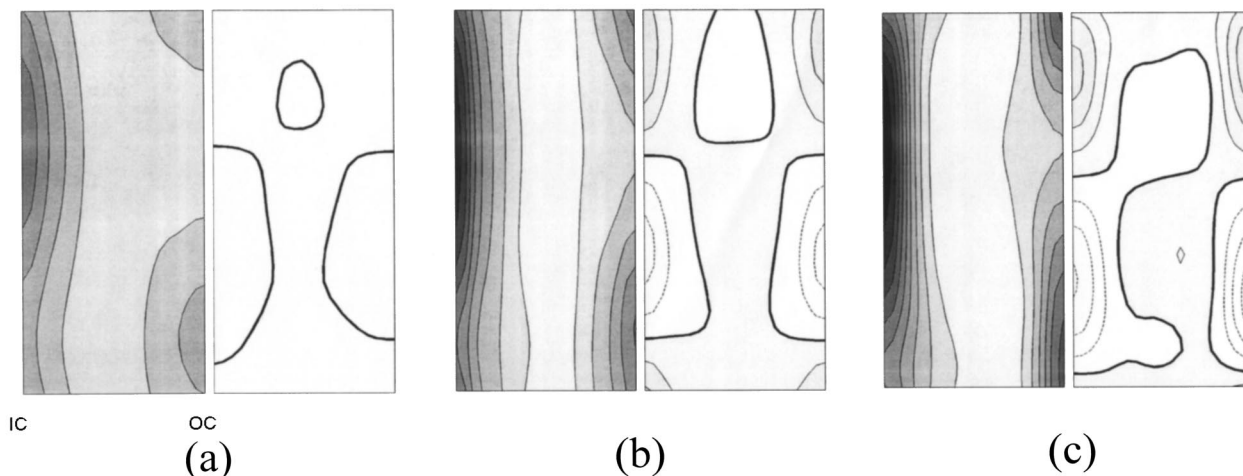


FIG. 11. Azimuthally averaged shear stress in a meridional plane. (a) $\varepsilon=0.28$, (b) $\varepsilon=1.48$, (c) $\varepsilon=5.03$. In each part, the left plane is the azimuthal shear stress, $\tau_{r\theta}d/\mu r_i\Omega$, and the right plane is the axial shear stress, $\tau_{rz}d/\mu r_i\Omega$. Bold solid contours are zero shear stress. Solid contours are positive and dashed contours are negative shear stress. The contour spacing is 0.5 for azimuthal shear stress ($\tau_{r\theta}$) and 0.2 for axial shear stress (τ_{rz}).

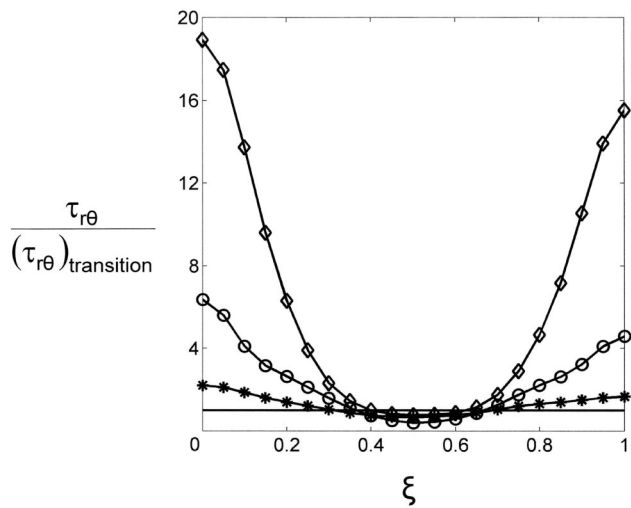


FIG. 12. Axially and azimuthally averaged azimuthal shear stress ($\tau_{r\theta}$) normalized by the local shear stress at transition to Taylor vortex flow at $\varepsilon = 0$; (*) $\varepsilon = 0.28$; (O) $\varepsilon = 1.48$; (\diamond) $\varepsilon = 5.03$. Solid horizontal line represents stable flow.

der rotation and are responsible for preventing particles suspended in a fluid from coming in close contact with the pores of the inner cylindrical filter surface in the application of rotating filtration, which we briefly discuss later. The third component of shear, $\tau_{\theta z}$, which we do not discuss further because it is not particularly helpful in understanding the flow, is half the magnitude of τ_{rz} and an order of magnitude smaller than $\tau_{r\theta}$.

The instantaneous dimensionless shear stress components $\tau_{rz}d/\mu r_i\Omega$ and $\tau_{r\theta}d/\mu r_i\Omega$ are shown in Fig. 10 at the time instants shown in Fig. 7, where μ is the dynamic viscosity. The gray scale is adjusted so that larger values of shear stress are darker, and values of shear stress with opposite sign are white with dashed contours. The same gray scale is used for all three Reynolds numbers to allow easy comparison. At all three Reynolds numbers, regions of high-

est azimuthal shear stress, $\tau_{r\theta}$, correspond to regions of radial inflow impinging on the inner cylinder. In this region slow fluid from near the outer cylinder is brought inward by the radial flow resulting in high radial gradients of the azimuthal velocity. For the highest Reynolds number, the shear stress at the inner cylinder for an inflow boundary is twice that for an outflow boundary. The shear at positions where radial outflow impinges on the outer cylinder also have high shear, though not as high as where inflow impinges on the inner cylinder. At the outer cylinder, the shear at an outflow boundary is more than three times that for an inflow boundary at the highest Reynolds number. The azimuthal shear stress is lowest in the middle of the annulus, where the azimuthal velocity profile flattens as a result of the transport of azimuthal momentum by the vortices.^{9,13} The axial shear stress, τ_{rz} , is not nearly as strong as the azimuthal shear stress. It is highest near the walls at axial positions aligned with the vortex centers. (Although the gray scale for τ_{rz} is identical to that for $\tau_{r\theta}$, the contours are spaced more closely.) Of course, the axial shear stress changes sign along the cylinder walls, depending on whether the axial flow at the wall is upward or downward.

Because of the undulation of the wavy vortices, the axial locations of highest shear stress along the cylinder walls depend on the phase of the vortices. Thus, it is useful to consider the time-averaged shear stress, shown in Fig. 11. The averaged azimuthal shear stress is more uniform in the axial direction than the instantaneous shear stress. Consequently, there are no local regions that are exposed to substantially higher shear stresses than other regions. The averaged axial shear stress is not as uniform along the cylinder walls, because some axial positions always have a net downward or upward flow. This is a consequence of the magnitude of the undulation of the vortices being less than the vortex size. However, the magnitude of the axial shear stress is substantially less than that of the azimuthal shear.

Although contours of the dimensionless shear stress are instructive, they do not display the increase in the magnitude

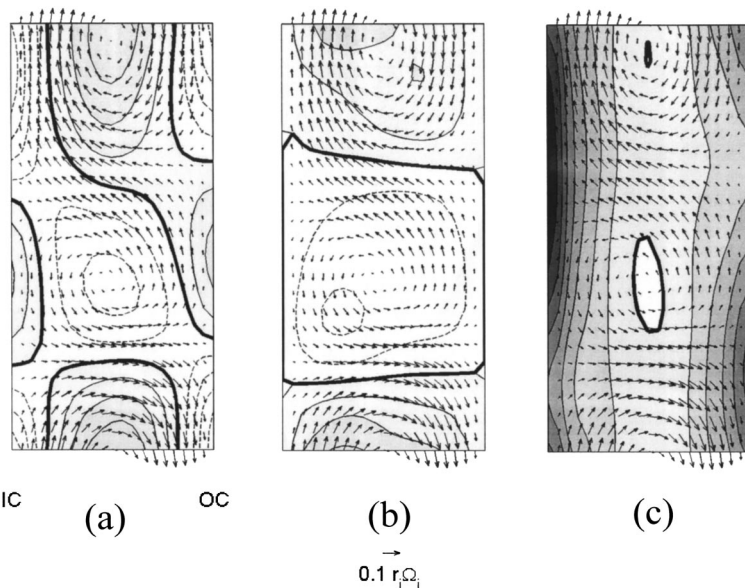


FIG. 13. Vorticity in a meridional plane for $\varepsilon = 1.48$. (a) $\omega_{\theta}d/r_i\Omega$, (b) $\omega_r d/r_i\Omega$, (c) $\omega_z d/r_i\Omega$. The contour line spacing is 0.1 for ω_{θ} , 0.2 for ω_r , and 0.5 for ω_z . Solid contours are positive vorticity, dashed contours are negative vorticity. Bold solid contours are zero vorticity.

of the dimensional shear stress with increasing Reynolds number. In Fig. 12, the azimuthally and axially averaged azimuthal shear stress is normalized by the local azimuthal shear stress at the transition from nonvortical flow ($\varepsilon=0$). At the inner cylinder the shear stress increases much faster than the rotational speed. For example, at $\varepsilon=5.03$, the rotational speed has increased by a factor of 6, but the shear stress at the inner cylinder has increased by a factor of 19 due to the redistribution of the azimuthal momentum by the vortical flow. The normalized shear stress is nearly as high at the outer cylinder. However, the shear stress in the middle of the annulus is actually lower than it is for $\varepsilon=0$ at all Reynolds numbers. This result has significant impact on biomedical and biotechnological applications of vortical Couette devices, where the cells that are being processed are often quite susceptible to damage by high shear—even though the shear is high at the walls of the device, the shear in the middle of the annulus is quite small.

The shear stress and vorticity are closely related, but it is still interesting to consider the vorticity, shown in Fig. 13 for $\varepsilon=1.48$ where the shading is darkest for the most positive vorticity and lightest for negative vorticity. Consider first the azimuthal vorticity in Fig. 13(a). The largest azimuthal vorticity coincides with the vortical motion, as would be expected, with little azimuthal vorticity between vortices. Regions of high radial vorticity extend across the entire annulus with the vorticity changing sign approximately at boundaries between vortices, as shown in Fig. 13(b). This boundary corresponds to the shear layer between vortices evident in Fig. 9. As expected, the axial vorticity shown in Fig. 13(c) is an order of magnitude larger than the other components of vorticity owing to the strong radial gradient of the azimuthal velocity at the walls. However, the radial transport of the axial vorticity due to the vortical flow is clearly evident in the curved contours at the inflow and outflow boundaries.

IV. CONCLUSIONS

Previous studies of cylindrical Couette flow have been incomplete in addressing the velocity field for wavy flow due primarily to the difficulty in making such measurements. We have made extensive PIV measurements in meridional and latitudinal planes that have enabled us to construct a time-resolved, three-dimensional field of all three velocity components at three Reynolds numbers for wavy vortical flow.

The vortices strengthen with increasing Reynolds number, and the azimuthal velocity profile at a particular axial location depends strongly on the fluid transport by the vortices. This results in an azimuthal velocity deficit at inflow regions and a velocity surplus at outflow regions. Interestingly, the azimuthal velocity deficit at inflow regions is greater than the velocity surplus at outflow regions. However, it has been shown that the gradient near the outer cylinder is not as steep as that near the inner cylinder and that the deviation of the velocity profile from nonvortical is not as severe near the outer cylinder as near the inner cylinder.^{9,13} The consequence is that the azimuthal velocity is augmented only near the outer cylinder in outflow regions, whereas it is diminished in a much larger region including

the inflow region and near the inner cylinder in the outflow region. Thus, there is a significant asymmetry in the azimuthal flow between the inflow and outflow regions.

Of course, the waviness of the vortices results in substantial variation in the azimuthal velocity in any given latitudinal plane, particularly near a vortex center. In addition, relatively strong axial flows carry fluid along the length of the annulus. This is a very different view of wavy vortex flow than the simplistic ideal of independent, wavy, toroidal vortex tubes. Instead, fluid flows in continuous axial streams that extend axially through the entire stack of wavy vortices along the length of the annulus. These axial streams wind around the vortices from the inner cylinder to the outer cylinder and also wind azimuthally about one-half wavelength and back. The combination of the vortical flow and these axial streams suggests significantly enhanced mixing via chaotic advection.

The azimuthal velocity near the centers of the vortex is quite similar to the traveling azimuthal wave velocity. This suggests that the waviness that is apparent both visually and via spectra of the velocity field is related to the motion of the vortex centers. This is especially interesting given that no clear explanation of the origin of the waviness has been put forth to date. Marcus¹³ suggested that the waviness is “caused by a local, inviscid, centrifugal instability of the outflow boundary.” On the other hand, Jones¹⁴ proposed that “it is the azimuthal jets which destabilize the axisymmetric flow.” These azimuthal jets are generated by the strong radial flows at the inflow and outflow boundaries. As a result, “the onset of wavy vortices occurs close to the onset of axisymmetric vortices for narrow gaps.” Our results in Fig. 9 show relatively strong shear layers in the azimuthal velocity compared to the radial inflow and outflow shear layers between the vortices. These results suggest that the azimuthal waviness is more likely related to an instability in the azimuthal velocity profile as proposed by Jones.

Finally, the shear stress distribution reflects the transport of fluid by the vortices. Near the inner and outer cylinders, the shear stress is quite large, especially at the highest Reynolds numbers. In the middle of the annulus, the shear stress is less than it would be if the flow were not vortical. This result is particularly important with regard to rotating filtration devices used in biological separations in which blood or a biosuspension in the annulus is filtered using a porous inner cylinder. The high shear near the inner cylinder probably acts to prevent plugging of the pores of the inner cylinder with cells, while the cells in the middle of the annulus are exposed only to a very low shear. The strong mixing related to the vortical motion and transport between vortices results in cells only being exposed to the highest shear for a very short time.

ACKNOWLEDGMENTS

This work was supported by the National Science Foundation. We thank Dr. Steven T. Wereley of Purdue University for several useful discussions during the course of this research.

- ¹G. I. Taylor, "Stability of a viscous liquid contained between two rotating cylinders," *Philos. Trans. R. Soc. London, Ser. A* **223**, 289 (1923).
- ²E. L. Koschmieder, *Benard Cells and Taylor Vortices* (Cambridge University Press, Cambridge, 1993).
- ³R. C. DiPrima and H. L. Swinney, "Instabilities and transition in flow between concentric rotating cylinders," in *Topics in Applied Physics, Hydrodynamic Instabilities and the Transition to Turbulence*, edited by H. L. Swinney and J. P. Gollub (Springer, Berlin, 1985), pp. 139–180.
- ⁴K. Kataoka, "Taylor vortices and instabilities in circular Couette flows," in *Encyclopedia of Fluid Mechanics*, edited by N. P. Chermisnoff (Gulf, Houston, 1986), Vol. 1, pp. 237–273.
- ⁵R. J. Donnelly, "Taylor–Couette flow: The early days," *Phys. Today* **44** (11), 32 (1991).
- ⁶J. P. Gollub and M. H. Freilich, "Optical heterodyne test of perturbation expansions for the Taylor instability," *Phys. Fluids* **19**, 618 (1976).
- ⁷T. Berland, T. Jøssang, and J. Feder, "An experimental study of the connection between the hydrodynamic and phase-transition descriptions of the Couette–Taylor instability," *Phys. Scr.* **34**, 427 (1986).
- ⁸R. M. Heinrichs, D. S. Cannell, G. Ahlers, and M. Jefferson, "Experimental test of the perturbation expansion for the Taylor instability at various wavenumbers," *Phys. Fluids* **31**, 250 (1988).
- ⁹S. T. Wereley and R. M. Lueptow, "Azimuthal velocity in supercritical circular Couette flow," *Exp. Fluids* **18**, 1 (1994).
- ¹⁰A. Davey, "The growth of Taylor vortices in flow between rotating cylinders," *J. Fluid Mech.* **14**, 336 (1962).
- ¹¹S. T. Wereley and R. M. Lueptow, "Spatio-temporal character of supercritical circular Couette flow," *J. Fluid Mech.* **364**, 59 (1998).
- ¹²D. Coles, "Transition in circular Couette flow," *J. Fluid Mech.* **21**, 385 (1965).
- ¹³P. S. Marcus, "Simulation of Taylor–Couette flow. Part 2. Numerical results for wavy-vortex flow with one travelling wave," *J. Fluid Mech.* **146**, 65 (1984).
- ¹⁴C. A. Jones, "The transition to wavy Taylor vortices," *J. Fluid Mech.* **157**, 135 (1985).
- ¹⁵K. T. Coughlin and P. S. Marcus, "Modulated waves in Taylor–Couette flow: Part 2. Numerical simulation," *J. Fluid Mech.* **234**, 19 (1992).
- ¹⁶J. P. Gollub and H. L. Swinney, "Onset of turbulence in a rotating fluid," *Phys. Rev. Lett.* **35**, 927 (1975).
- ¹⁷A. Brandstater and H. L. Swinney, "Strange attractors in weakly turbulent Couette–Taylor flow," *Phys. Rev. A* **35**, 2207 (1987).
- ¹⁸Y. Takeda, W. E. Fischer, and J. Sakakibara, "Decomposition of the modulated waves in a rotating Couette system," *Science* **263**, 502 (1994).
- ¹⁹K. Kose, "Spatial mapping of velocity power spectra in Taylor–Couette flow using ultrafast NMR imaging," *Phys. Rev. Lett.* **72**, 1467 (1994).
- ²⁰D. Riechelmann and K. Nanbu, "Three-dimensional simulation of wavy Taylor vortex flow by direct simulation Monte Carlo method," *Phys. Fluids* **9**, 811 (1997).
- ²¹C. L. Streett and M. Y. Hussaini, "A numerical simulation of the appearance of chaos in finite-length Taylor–Couette flow," *Appl. Numer. Math.* **7**, 41 (1991).
- ²²S. GhoshMoulic and L. S. Yao, "Taylor–Couette instability of travelling waves with a continuous spectrum," *J. Fluid Mech.* **324**, 181 (1996).
- ²³K. A. Meyer, "Time-dependent numerical study of Taylor vortex flow," *Phys. Fluids* **10**, 1874 (1967).
- ²⁴K. A. Meyer, "Three-dimensional study of flow between concentric rotating cylinders," *High-Speed Computing in Fluid Dynamics: Phys. Fluids Suppl. II* **12**, II-165 (1969).
- ²⁵R. Meyer-Spasche and H. B. Keller, "Computations of the axisymmetric flow between rotating cylinders," *J. Comput. Phys.* **35**, 100 (1980).
- ²⁶A. K. Majumdar and D. B. Spalding, "Numerical computation of Taylor vortices," *J. Fluid Mech.* **81**, 295 (1977).
- ²⁷C. A. Jones, "Nonlinear Taylor vortices and their stability," *J. Fluid Mech.* **102**, 249 (1981).
- ²⁸R. D. Moser, P. Moin, and A. Leonard, "A spectral numerical method for the Navier–Stokes equations with applications to Taylor–Couette flow," *J. Comput. Phys.* **52**, 524 (1983).
- ²⁹H. Fasel and O. Booz, "Numerical investigation of supercritical Taylor-vortex flow for a wide gap," *J. Fluid Mech.* **138**, 21 (1984).
- ³⁰W. Schroder and H. B. Keller, "Wavy Taylor-vortex flows via multigrid-continuation methods," *J. Comput. Phys.* **91**, 197 (1990).
- ³¹R. P. Dring, "Sizing criteria for laser anemometry particles," *ASME J. Fluids Eng.* **104**, 15 (1982).
- ³²C. E. Willert and M. Gharib, "Digital particle image velocimetry," *Exp. Fluids* **10**, 181 (1991).
- ³³A. Recktenwald, M. Lücke, and H. W. Müller, "Taylor vortex formation in axial through-flow: Linear and weakly nonlinear analysis," *Phys. Rev. E* **48**, 4444 (1993).
- ³⁴C. D. Andereck, S. S. Liu, and H. L. Swinney, "Flow regimes in a circular Couette system with independently rotating cylinders," *J. Fluid Mech.* **164**, 155 (1986).
- ³⁵W. S. Edwards, S. R. Beane, and S. Varma, "Onset of wavy vortices in the finite-length Couette–Taylor problem," *Phys. Fluids A* **3**, 1510 (1991).
- ³⁶W. S. Edwards, R. P. Tagg, B. C. Dornblaser, and H. L. Swinney, "Periodic traveling waves with nonperiodic pressure," *Eur. J. Mech. B/Fluids* **10**, 205 (1991).
- ³⁷G. S. Bust, B. C. Dornblaser, and E. L. Koschmieder, "Amplitudes and wavelengths of wavy Taylor vortices," *Phys. Fluids* **28**, 1243 (1985).
- ³⁸H. A. Snyder and R. B. Lambert, "Harmonic generation in Taylor vortices between rotating cylinders," *J. Fluid Mech.* **26**, 545 (1966).
- ³⁹D. S. Broomhead and S. C. Ryrie, "Particle paths in wavy vortices," *Nonlinearity* **1**, 409 (1988).
- ⁴⁰S. C. Ryrie, "Mixing by chaotic advection in a class of spatially periodic flows," *J. Fluid Mech.* **236**, 1 (1992).
- ⁴¹P. Ashwin and G. P. King, "A study of particle paths in non-axisymmetric Taylor–Couette flows," *J. Fluid Mech.* **338**, 341 (1997).
- ⁴²M. Rudman, "Mixing and particle dispersion in the wavy vortex regime of Taylor–Couette flow," *AIChE J.* **44**, 1015 (1998).
- ⁴³M. Rudolph, T. Shinbrot, and R. M. Lueptow, "A model of mixing and transport in wavy Taylor–Couette flow," *Physica D* **121**, 163 (1998).
- ⁴⁴G. P. King, G. Rowlands, M. Rudman, and A. N. Yannacopoulos, "Predicting chaotic dispersion with Eulerian symmetry measures: Wavy Taylor-vortex flow," *Phys. Fluids* **13**, 2522 (2001).
- ⁴⁵I. Mezic, "Chaotic advection in bounded Navier–Stokes flows," *J. Fluid Mech.* **431**, 347 (2001).
- ⁴⁶A. Akonur and R. M. Lueptow, "Chaotic mixing and transport in wavy Taylor Couette flow," *Physica D* **167**, 183 (2002).
- ⁴⁷G. P. King, Y. Li, W. Lee, H. L. Swinney, and P. S. Marcus, "Wave speeds in wavy Taylor-vortex flow," *J. Fluid Mech.* **141**, 365 (1984).